

# The Numerical Investigation of Hydrogen Detonation Propagating in Semi-confined Layers

Shunsuke SHIGEOKA<sup>1</sup>, Akiko MATSUO<sup>1</sup>  
Akira KAWASAKI<sup>2</sup>, Ken MATSUOKA<sup>2</sup>, Jiro KASAHARA<sup>2</sup>

<sup>1</sup>Department of Mechanical Engineering, Keio University  
3-14-1 Hiyoshi, Kohoku-ku, Yokohama, Kanagawa 223-8522, Japan

<sup>2</sup>Department of Aerospace Engineering, Nagoya University  
Furo-cho, Chikusa-ku, Nagoya, Aichi 464-8603, Japan

## 1 Introduction

Hydrogen is sustainable and clean energy source because it does not emit carbon dioxide when it combusts. On the other hand, the safety of hydrogen needs to be paid attention for its low ignition energy. Considering hydrogen leakage in a building as one accidental situation, it is mixed with air and accumulated around the ceiling because of the low density. In the other words, the combustible mixture layer is produced between a rigid wall and inert layer. This system is called as semi-confined layers in this paper compared with confined geometry for example a channel. Detonation is one of the premixed combustions induced by shock waves. The pressure and temperature after the detonation is higher than deflagration. When detonation occurs accidentally, not only the building, but surroundings may be damaged seriously. Therefore, knowledges about the characteristics of detonation in semi-confined layers is required.

Detonation propagates in semi-confined layers where the height of hydrogen-air layer is 3 times as high as the cell width [1]. The wave front of gaseous detonation in semi-confined layers has global curvature because of divergence of streamlines as same as condensed phase detonation. For the detonation with global curvature, Wood and Kirkwood [2] proposed one-dimensional steady analysis. Reynaud et al. [3] simulates detonation in semi-confined layers using one-step irreversible Arrhenius reaction model. They concluded that the Favre averaged structure of detonation along the wall corresponds to Wood and Kirkwood model in the low activation energy case. However, in the high activation energy case the velocity deficit does not correspond to the model. Houim et al. [4] numerically investigate the effect of the acoustic impedance ratio between combustible and inert gas layer by changing the temperature of inert gas. The structure of the oblique shock and detonation varies by the acoustic impedance ratio.

In the experiment of detonation in semi-confined layers, the densities of combustible and inert layers are different because the components are not same. However, one-step irreversible model is used in the previous numerical studies which does not consider the difference of components. In this report, detonation in semi-confined layers is investigated by utilizing detailed chemical kinetics. The velocity deficit and averaged structure are discussed especially in stable section.

## 2 Numerical Setup

Figure 1 (a) shows a schematic image of a calculation target. Detonation propagates left to right in the layers of combustible and inert gas. The component of combustible gas is  $\text{H}_2 : \text{O}_2 : \text{N}_2 = 2 : 1 : 1.5$  and the component of inert gas is  $\text{O}_2 : \text{N}_2 = 1 : 1.5$  in a molar ratio. The temperature of the both gasses are 298 K and the pressure is 1 atm. The grid resolution is  $6 \mu\text{m}$ . About 13 grid points include in half reaction length  $l_{1/2}$ . Figure 1 (b) shows the initial and boundary condition. Developed two-dimensional detonation in channel is used for initial condition. The height of combustible layer  $h$  is a parameter. For reducing calculation cost, the computational grid is moved to right when the detonation approaches the right boundary. For the first 50000 step, second-order scheme is used for discretizing convective terms to calculate stably. This operation does not affect the conclusion because a quasi-steady state is only focused. In following results, the time changing fifth-order scheme is set as 0 s. CJ velocity  $D_{\text{CJ}}$  is 2284 m/s, the effective activation energy  $E_a / RT_{\text{vN}}$  is 6.514 and the half reaction length  $l_{1/2}$  is 78.98  $\mu\text{m}$ .

The governing equations are two-dimensional compressible Euler equation with the conservation equations of 9 species ( $\text{H}_2$ ,  $\text{O}_2$ , O, H, OH,  $\text{H}_2\text{O}$ ,  $\text{HO}_2$ ,  $\text{H}_2\text{O}_2$ ,  $\text{N}_2$ ). The ideal gas law is utilized to close the equations, and thermodynamic parameter is calculated by NASA polynomials [5]. The convective and source terms are separated by 1<sup>st</sup> order fractional time splitting. To discretize and integrate the convective term, AUSM-DV scheme [6] with fifth-order finite volume based WENO [7] and third-order TVD Runge-Kutta method are applied. The source term is integrated by Multi-Time Scale method [8] to avoid stiffness problem. Chemical reaction model includes 9 species and 20 elementary reactions [9].

## 3 Results and Discussions

Figure 2 shows numerical maximum pressure histories of 2 different cases. Figure 2 (a) is  $h/l_{1/2} = 152$  case, and Figure 2 (b) is  $h/l_{1/2} = 182$  case. In the lower layer height case, cellular structure is very irregular because the transverse waves do not reflect enough at the boundary between inert and combustible gases

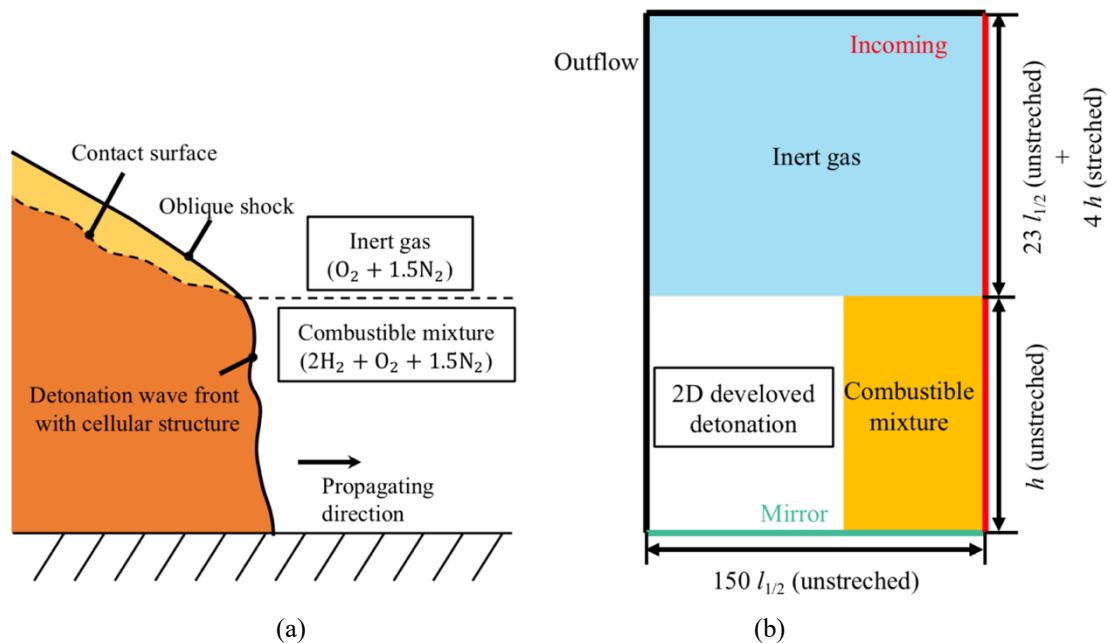


Figure 1. Schematic image (a) calculation target (b) calculation condition

(see Figure 2 (a)). Around  $x/l_{1/2} = 1100$ , two triple points collide at the top of combustible layer. However, the triple point which propagate toward the bottom does not have enough strength and detonation quenches. In the higher layer height case, the cell width is small, and detonation propagates over  $3000 l_{1/2}$  (see Figure 2 (b)). In both cases, the reflection of triple points is sometimes confirmed because the acoustic impedance ratio between the inert and combustible layers is different.

Figure 3 shows the history of the number of triple points. The horizontal axis means the position which the bottom of detonation front reaches. While  $x$  is from 0 to  $2000 l_{1/2}$ , the number of triple points does not

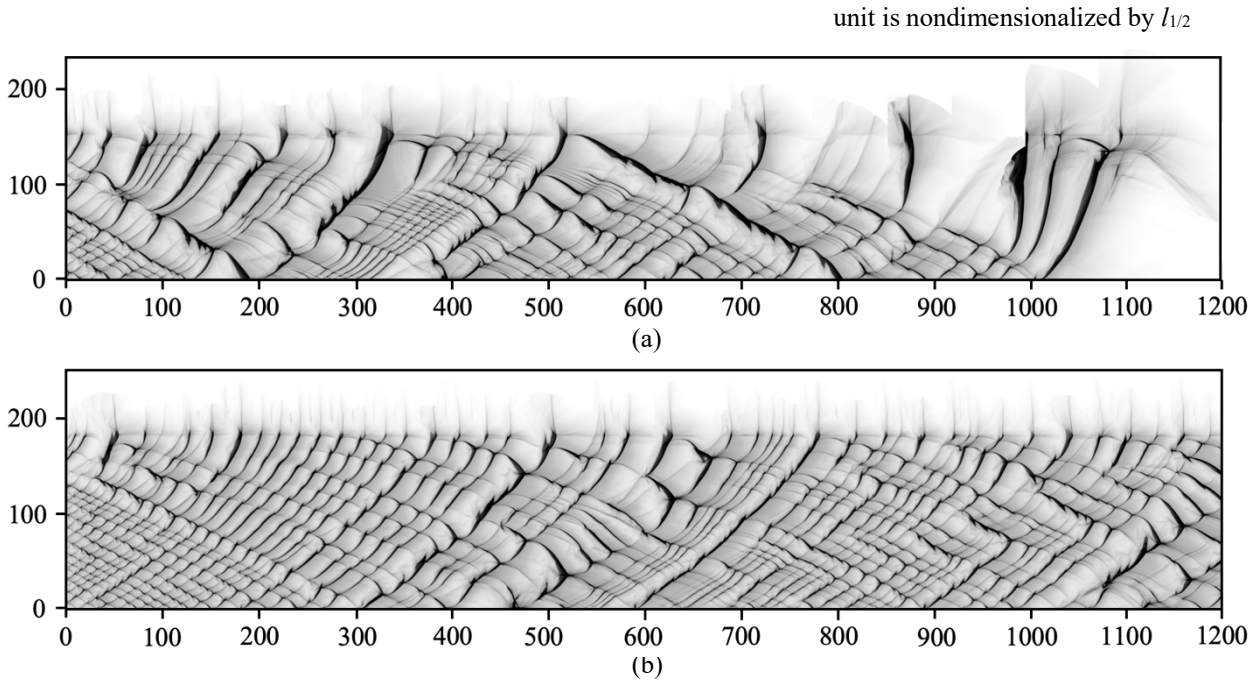


Figure 2. Numerical maximum pressure history (a) Lower layer height ( $h/l_{1/2} = 152$ )  
(b) Higher layer height ( $h/l_{1/2} = 182$ )

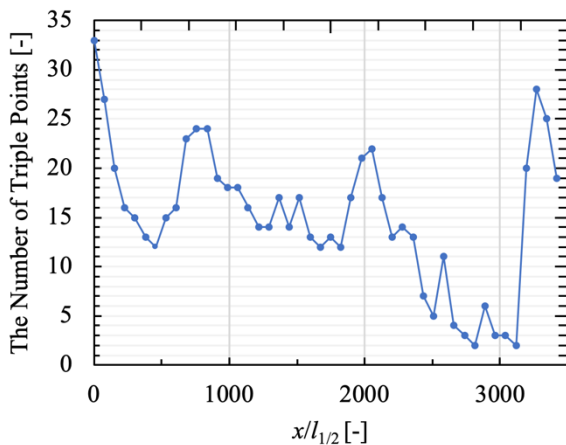


Figure 3. The history of the number of triple points  
( $h/l_{1/2} = 182$ )

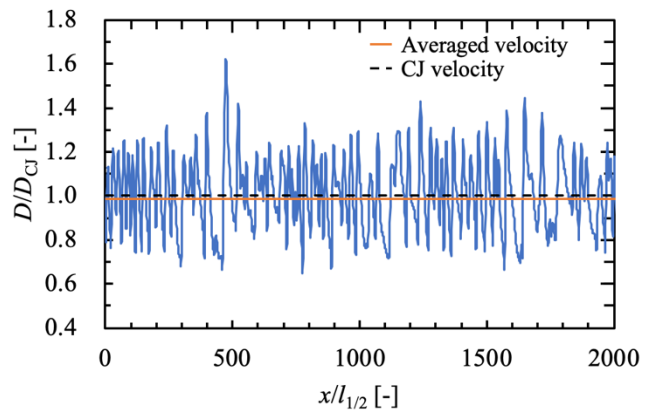


Figure 4. The history of the velocity at the bottom  
( $h/l_{1/2} = 182$ )

fluctuate dramatically. However, around  $x/l_{1/2} = 2300$ , the number of triple points decreases to one digit. In the following data, the stable section,  $0 < x/l_{1/2} < 2000$ , is treated in order to lessen the effect of cellular behavior and focus on the averaged structure. Figure 4 presents the history of the velocity at the bottom line. The velocity is calculated by differentiating the position of incident shock utilizing Savitzky-Golay filter [10]. The velocity fluctuation represents the fluctuation in cellular periods and the cellular irregularity. In this section, the averaged velocity of detonation is  $0.985 D_{CJ}$ .

Figure 5 shows temperature and OH mass fraction fields when the detonation reaches about  $x/l_{1/2} = 750$ . In the statement of this paper, the sonic speed ratio between the inert and combustible layers are not different excessively. Therefore, the oblique shock does not separate from the detonation front as the previous study [4]. The detonation front inclines because the confined effect is not enough at the top of combustible layer and flow path is expanded. The transverse waves are located irregularly, and the unburned gas pocket remains behind the detonation front.

Figure 6 presents the instant and averaged shape of detonation front. The averaging method is arithmetic mean of the position data along the same  $y$  line. The instant position of detonation front is concentrated upon the averaged position. In conjunction with the result of Figure 3, detonation exhibits the quasi-steady behavior. The curvature of detonation front is obtained by approximating the averaged position with 3<sup>rd</sup> and 5<sup>th</sup> degree approximating polynomial (see Figure 7). Both approximating polynomials correspond well to the original averaged positions and their R-squared values correspond to 1 with an accuracy of  $10^{-4}$ . In the area higher than  $y = 50 l_{1/2}$ , the curvatures of detonation front are different from each other because the second-order differential value included in curvature is strongly affected by the order of approximating polynomial. However, in the area lower than  $y = 50 l_{1/2}$ , the curvatures are near zero. Therefore, the detonation in the bottom region is able to propagate CJ velocity from the point of view of the loss due to curvature. Figure 8 presents the Favre averaged flow fields. The data for Favre averaging process is taken from the shock front while  $0 < x < 2000 l_{1/2}$ . In addition, the Favre averaged data is arranged along

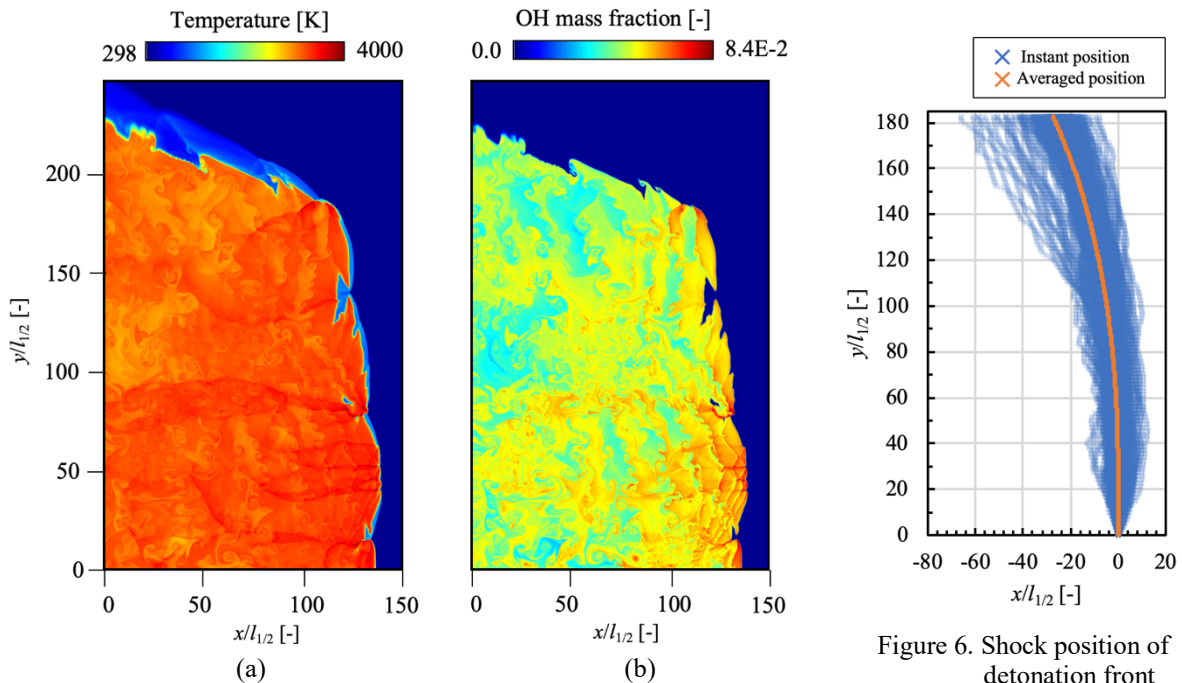


Figure 5. Instant flow field (a) temperature (b) OH mass fraction ( $h/l_{1/2} = 182$ )

Figure 6. Shock position of detonation front ( $h/l_{1/2} = 182$ )

the averaged position in Figure 6. The averaged stream lines around the bottom are parallel to the bottom boundary (see Figure 8 (a)). On the other hand, the stream lines incline upward in the area higher than  $y = 50 l_{1/2}$ . The inclination is caused by the slope of detonation front. In the region higher than  $x = 40 l_{1/2}$  and  $y = 150 l_{1/2}$ , velocity magnitude increases clearly. The increment is caused by expansion waves which are generated by expansion of stream line. The Figure 8 (b) shows Mach number distribution in the shock fixed frame and the sonic line along the stream line. The distance between the detonation front and sonic line is longest around the bottom and decrease as the  $y$  value increases. Figure 8 (c) presents  $H_2$  mass fraction, sonic line and the equilibrium value of  $H_2$  mass fraction in ZND solution. In the region under  $y = 130 l_{1/2}$ , the

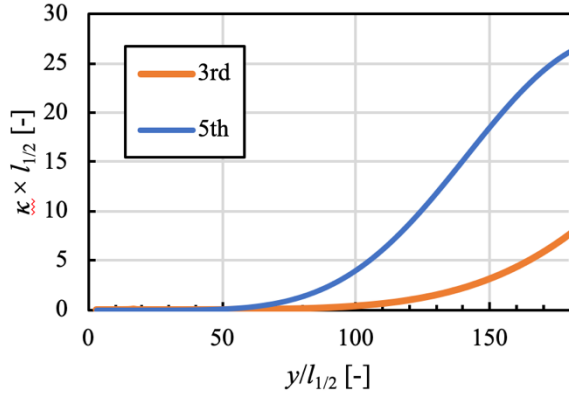


Figure 7. Relation between the order of approximating polynomial and the curvature ( $h/l_{1/2} = 182$ )

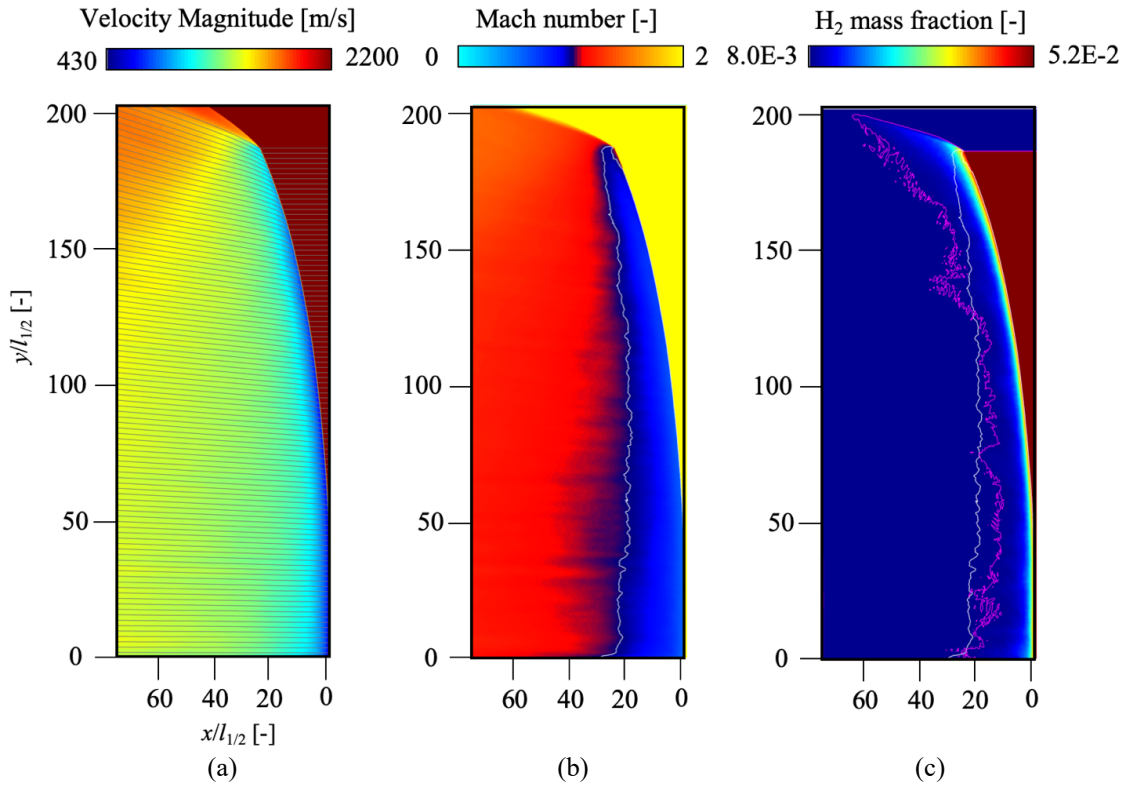


Figure 8. Favre averaged flow field (a) Velocity magnitude and stream line (gray line) (b) Mach number and sonic line (white line) (c)  $H_2$  mass fraction and the equilibrium value (pink line) ( $h/l_{1/2} = 182$ )

equilibrium value is inside the sonic line. Therefore, the detonation is enough driven by the chemical reaction energy. However, around the top of detonation, the equilibrium value line exists outside of the sonic line. The fact that unburned gas pockets constantly occurs around the top of detonation is indicated. A part of the energy which is released behind the sonic line is not able to contribute the detonation front. The velocity deficit along the bottom line in stable section is caused by the short of chemical energy which is affect the detonation front.

## 4 Conclusions

Hydrogen detonation propagates in the combustible and inert layers is investigated. The critical height where detonation propagates is  $h/l_{1/2} = 182$ . A part of the transverse waves is reflected at the boundary of layers and prevent the number of triple points from decreasing immediately. The shape of detonation front at the bottom in stable section is normal to the bottom boundary and there is no curvature. The averaged velocity deficit from CJ velocity is about 1.5 %. The deficit is not able to be explained by the loss of curvature. Favre averaged flow field while stable section shows the continuous existence of unburned  $H_2$  which locates behind the sonic line along flow path. Its area is around the top of combustible layer. Around the bottom of combustible layer,  $H_2$  reaches equilibrium value in one-dimensional model within the averaged sonic line. Therefore, the bottom part of detonation has an important role to drive the detonation as a whole.

## References

- [1] W. Rudy, K. Dziubanii, M. Zbikowski, A. Teodorczyk. (2016). Experimental Determination of Critical Conditions for Hydrogen-Air Detonation Propagation in Partially Confined Geometry. *Int. J. Hydrogen Energy*. 42: 7366.
- [2] W. W. Wood, J. G. Kirkwood. (1954). Diameter Effect in Condensed Explosives. the Relation between Velocity and Radius of Curvature of the Detonation Wave. *J. Chem. Phys.* 22: 1920.
- [3] M. Reynaud, F. Viro, A. Chinnayya. (2017). A computational study of the interaction of gaseous detonations with a compressible layer. *Phys. Fluids*. 29: 1
- [4] R. Houim, R. T. Flevinsohn. (2017). The influence of acoustic impedance on gaseous layered detonations bounded by an inert gas. *Combust. Flame*. 179: 185.
- [5] B. J. McBride, A. R. Martin. (1993). Coefficients for Calculating Thermodynamic and Transport Properties of Individual Species”, NASA Technical Memorandum. 4513: 10.
- [6] Y. Wada, M. S. Liou. (1997). An accurate and roust flux splitting scheme for shock and contact discontinuities. *J. Sci. Comput.* 18: 633.
- [7] G. S. Jiang, C. W. Shu. (1996). Efficient Implementation of Weighted ENO Schemes. *J. Comput. Phys.* 122: 202.
- [8] X. Gou, W. Sun, Z. Chen, Y. Ju. (2010). A Dynamic Multi-Timescale Method for Combustion Modeling with Detailed and Reduced Chemical Kinetic Mechanisms. *Combust. Flame*. 157: 1111.
- [9] Z. Hong, D. F. Davidson, R. K. Hanson. (2011). An Improved  $H_2 / O_2$  Mechanism Based on Recent Shock Tube / Laser Absorption Measurements. *Combust. Flame*. 158: 634
- [10] P. A. Gorry. (1991). General least-squares smoothing and differentiation of nonuniformly spaced data by the convolution method. *Anal. Chem.* 63: 534.